Cyclic deformation and lattice strain distribution of high Nb containing TiAl alloy

Jie Ding[a,b], Shan Shi[a], Zhili Dong [b], Junpin Lin[c], Yang Ren[d], Xiaodong Wu[a,b]*, Hui Chang[a]*, Lian Zhou[a]

[a] *Tech Institute for Advanced Materials, College of Materials Science and Engineering, Nanjing Tech University, Nanjing 210009, China*

[b] *School of Material Science and Engineering, Nanyang Technological University, 50 Nanyang Avenue, Singapore 639798, Singapore*

[c] *State Key Laboratory for Advanced Metals and Materials, University of Science and Technology Beijing, Beijing 100083, China*

[d] *X-ray Science Division, Advanced Photon Source, Argonne National Laboratory, Argonne, IL 60439, USA*

Abstract

Low cycle fatigue of lamellar TiAl with 8.5 at.% Nb was studied with a total strain amplitude of 0.28% at three temperatures: room temperature, 750 and 900 °C. At room temperature, the material exhibited cyclic hardening and the fracture mode was mainly interlamellar. At 750 and 900 °C, the material showed cyclic softening and the fracture mode was translamellar. The lattice strain in γ phase was almost tensile and larger tensile lattice strain in γ phase seems detrimental. Besides, opposite direction of $\{201\}_{\gamma}$ and $\{100\}_{\alpha 2}$ lead to crack propagation along α_2/γ interfaces. B2/β_o phase always suffered compressive lattice strain in the tests. The destruction of lamellar microstructure was the reason for colony refinement at 750 °C and 900 °C.

Keywords: TiAl alloys; low cycle fatigue; cyclic stress-strain behavior; recrystallization; phase transformation; fracture behavior

1. Introduction

γ-TiAl alloys are one of the most promising lightweight structural materials, due to their low density and excellent high temperature mechanical properties [1-5]. They have been investigated in order to replace nickel-based superalloys, for use in both the turbine and compressor stages of engines in the field of aerospace, automotive and

energy industries [6-8]. To date, the third generation γ-TiAl alloys containing high Nb addition, with higher oxidation and creep resistance, are expected to be served at higher operational stresses and temperatures, to 750 °C or higher, compared with the previous generation of TiAl-based alloys [9-11], which have received considerable attention in recent years. The properties of γ-TiAl in comparison with Ti6Al4V and Inconel 718 are summarized in Table 1.

Table 1 Properties of TiAl in comparison with Ti6Al4V and Inconel 718 [1, 4, 6, 8, 9]

Property	γ-TiAl	Ti6Al4V	Inconel 718
Density (g/cm^3)	3.9-4.2	4.4	8.2
Maximum operating temperature (°C)	750	315	650
RT-yield strength (MPa)	1265	880	1170
RT-ultimate tensile strength (MPa)	1334	950	1350
RT-ductility (%)	2.4	14	16
Thermal conductivity (W/mK)	16-26 (100-900 °C)	4-17 (300-800 °C)	11-22 (25-900 °C)
Specific 1000h rupture stress (MPa/g cm^{-3})	20-100 (600-800 °C)	45-150 (100-400 °C)	55-110 (500-600 °C)

As parts of aero and automotive combustion engines, γ-TiAl alloys are subjected to fluctuating or cyclic loading at high temperature. The occasional large mechanical or thermal transients during service may give rise to amount of plastic deformation, which is commonly referred to as low cycle fatigue (LCF). For such loading conditions, microstructure and mechanical properties should be maintained during service. The studies to capture microstructure evolution after low cycle fatigue of TiAl alloy have already been performed [12-14]. Furthermore, the relation between cyclic stress-strain (CSS) behavior and microstructure evolution was investigated [15-17]. However, the micro-mechanical behavior of high Nb-containing TiAl alloys after cyclic deformation have not been considered widely. In our previous study [18], the lattice strains have a big influence on fracture behavior. Large differences of the lattice strains in the γ phase and α_2 phase resulted in crack nucleated at and propagated along the α_2/γ lamellar interface. A viewpoint is also emerging that the fatigue performance of TiAl alloy couple with understanding of the residual lattice strain/stress and microstructure in cyclic failed samples at different service temperatures.

This paper will present information regarding the residual lattice strain/stress of high Nb containing TiAl alloy after low cycle fatigue at room temperature, 750, and 900 °C with a total strain amplitude of $\Delta\varepsilon_t/2 = \pm 0.28\%$. The microstructure evolution, the α_2/γ lamellar colony refinement, and fracture behaviors will be also investigated.

2. Experimental procedure

The high Nb-containing TiAl alloy with a nominal composition of Ti-45Al-8.5Nb-0.2W-0.2B-0.02Y (at. %) [18-22] investigated in this study was produced by a plasma arc cold hearth process with an ingot size of 730 × 340 ×900 mm. Cylindrical samples with a gage section of 14 mm in diameter and 100 mm in length were cut from the ingot by electro-discharge machining (EDM) process. To obtain the fully lamellar microstructure, cylindrical samples were heat treated within the single α phase field at 1340 °C for 24h under argon atmosphere, followed by furnace cooling. Button-ended cylindrical fatigue samples with a gauge diameter 6 mm, gauge length 32 mm, and total length 90 mm were prepared as shown in Fig. 1. Prior to fatigue tests, the final surface of the tested pieces was achieved by mechanical polishing, using the 2000 grit SiC papers, to minimize the effects of irregularities on fatigue lives. The strain-controlled low cycle fatigue tests referred to ASTM E606/E606M-12 <Standard Test Method for Strain-Controlled Fatigue Testing > were conducted on MTS 810 servohydraulic machine at room temperature, 750 °C and 900 °C in air. All the total strain amplitude was kept constant as well as strain rate of 5×10^{-3} s^{-1}. The signal was triangular, and the loading cycle was symmetrical ($R_\varepsilon = \varepsilon_{min}/\varepsilon_{max} = -1$). Three thermocouples were used to monitor the homogeneity and stability of the temperature during testing.

Microstructures after low cycle fatigue tests were examined on field emission scanning electron microscopy Zeiss SUPRA 55 instrument (SEM), using the backscattered electron mode (BSE) and secondary electron mode (SE). Sub-microstructures were examined on a Tecnai G^2 F30 instrument, and the thin foils were cut perpendicularly to the loading direction on the gage length of fatigue samples. Micro-strains were obtained by ex-situ synchrotron-based high-energy X-ray diffraction (HE-XRD) technique, which was conducted at the Advanced Photon Source, beamline 11 ID-C, at Argonne National Laboratory, IL, USA. The experimental setup was schematic represented in

Fig. 2. The distance from sample to a two-dimensional detector was approximately 2.5 m. The incident X-ray wavelength was 0.1173-Å, and the beam could be focused to a spot size of 50 ×50 μm. A ceria sample was tested for calibration, while an as-received sample (heat treated) was also measured to obtain the initial data. Debye rings were transferred into one-dimensional diffraction patterns by FIT2D software.

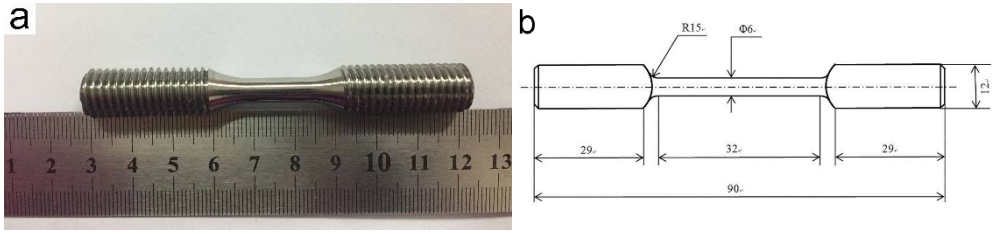

Fig. 1 (a) Actual solid specimen; (b) detailed dimensions of specimen (dimension in mm).

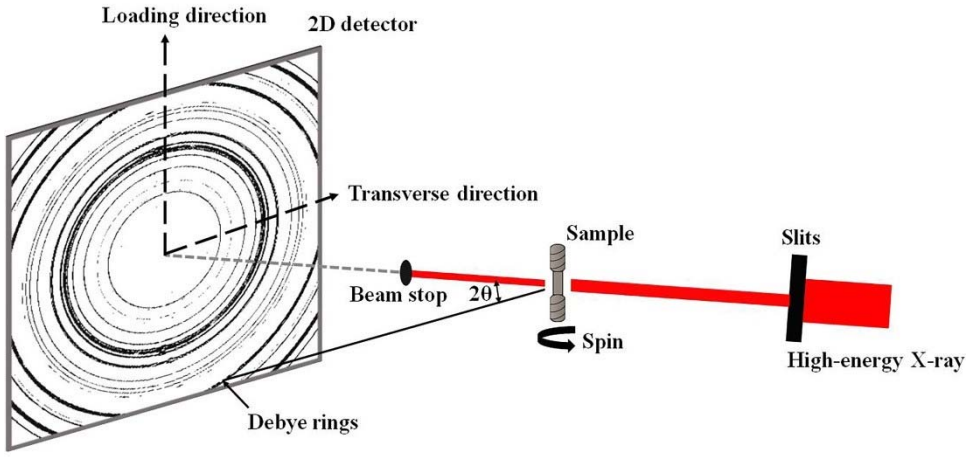

Fig. 2 Schematic representation of the experimental setup used for HE-XRD experiments on high Nb-containing alloy.

3. Results and discussion

3.1 Cyclic stress-strain behavior

Fig.3a presented the cyclic stress-strain (CSS) behavior of the fully lamellar high Nb-containing TiAl alloy, i.e., the variation of the stress amplitude $\Delta\sigma/2$ measured as a function of the number of cycles at room temperature, 750 °C, and 900 °C. The total strain amplitude of $\Delta\varepsilon_t/2 = \pm 0.28\%$ was selected to analyze the effect of the temperature on fatigue property. Accordingly, the material exhibited a slight cyclic hardening at room temperature, while a significant cyclic softening at 750 and 900 °C. However, the fatigue life of sample cyclic deformed at 900 °C was shorter than that of 750 °C. This

may mainly due to the higher accumulated plastic strain in the sample cyclic failed at 900 °C than at 750 °C, as showed in Fig. 3b. Fig.3b showed the plastic deformation accumulated in a cycle of the high-Nb containing TiAl alloy. The plastic strain amplitude $\Delta\varepsilon_p/2$ was a slight decrease at room temperature and increased at 750 °C and 900 °C. It was indicated that at room temperature, the material exhibited cyclic hardening, but cyclic softening at 750 °C and 900 °C. It seems that the investigated material was more suitable to serve at 750 °C, because the fatigue life was longer and the plastic strain amplitude was lower than that at room temperature and 900 °C. Plenty of studies have shown that cyclic hardening typically occurred in TiAl alloys at room temperature [23, 24], and cyclic softening was also observed at 850 °C with total strain amplitude of $\Delta\varepsilon_t/2 = \pm 0.28\%$ in our previous study [18], which was similar with the result in the present study.

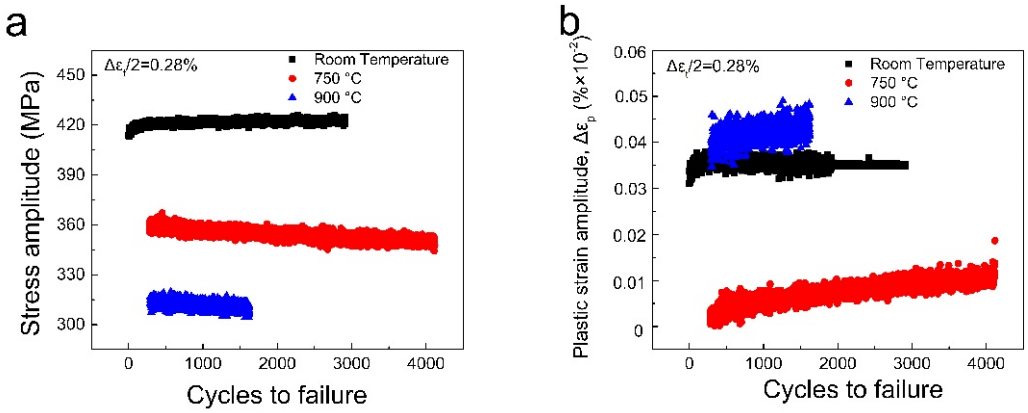

Fig. 3 Fully lamellar Ti-45Al-8.5Nb-0.2W-0.2B-0.02Y alloy cyclic deformed with total strain amplitude of $\Delta\varepsilon_t/2 = \pm 0.28\%$ at room temperature, 750 °C, and 900 °C: (a) cyclic stress-strain behavior, (b) accumulated plastic strain in a cycle.

3.2 Distribution of lattice strains after low cycle fatigue at evaluated temperatures

In order to understand the distribution of lattice strains, a gage length scan was performed on the failed high Nb-containing TiAl samples after cyclic deformation, with the scattering vector parallel to the loading direction (LD). The lattice strains measured by high-energy X-ray diffraction were phase-based strains, and were the average value in the X-ray beam focused spot size of 50 ×50 μm area. In order to involve more grains in the diffraction, fatigue samples were spinning during the HEXRD tests.

In this work, the ex-situ high-energy X-ray diffraction tests were conducted on 4 different samples, referred to the as-received sample, RT-0.28%, 750 °C-0.28%, and 900 °C-0.28%. The interplanar spacing of the undeformed TiAl alloy (the as-received sample), which referred as d_0 (Fig. 4a), was obtained from the sample after heat treatment and machined into the geometry mentioned in experimental procedure. Samples after cyclic deformation were failed almost at the middle of the gage length, and the d_0 values of the constituent phases were scanned along the same orientation and over the same length scale on the as-received sample. The d_{hkl}, which presented for the interplanar spacing of the $\{hkl\}$ plane, was obtained from samples under the given strain loading level at tested temperatures, and was calculated through Bragg's law, i.e., $\lambda=2 d_{hkl} \sin\theta_{hkl}$, where λ was the wavelength and θ_{hkl} was the diffraction angle of a Debye cone. Then the phase-based lattice strain ε_{hkl} were calculated by the equation of $\varepsilon_{hkl} = (d_{hkl}- d_0)/ d_0$.

The lattice strain distributions obtained with $\{201\}_\gamma$, $\{100\}_{\alpha2}$, and $\{220\}_{\beta o}$ reflections were shown in Fig. 4b-d. The positive values of the lattice strains indicated tensile lattice strains, whereas the negative values indicated compressive lattice strains. As can be seen from Fig. 4b, the lattice strains of $\{201\}_\gamma$ were fluctuated at zero and almost positive with a total strain amplitude of $\Delta\varepsilon_t/2 = \pm0.28\%$ at 750 and 900 °C, while the lattice strains of $\{100\}_{\alpha2}$ were almost compressive and fluctuated. Moreover, the values of lattice strains of γ phase was positive and larger in the sample cyclic deformed at 900 °C than that in samples cyclic deformed at room temperature and 750 °C. Similarly, larger compressive lattice stain in α_2 phase can be found in samples fatigued at 900 °C, as showed in Fig. 4c. It is may mainly due to the α_2/γ lamellae structure that the direction of lattice strains in α_2 and γ phase were opposite. This was also observed in the interrupted fatigue samples which cyclic deformed at 850 °C in our previous study. Furthermore, the lattice strains in β_o phase were always compressive at evaluated temperatures. It seemed that larger positive lattice strains in γ phase was detrimental to TiAl alloy, which resulted in a shorter fatigue life. As most successful application of residual stress was introduced into the surface layer of various components to improve their fatigue life [25–27], this result may be a guidance for TiAl alloys to take advantage

of the residual stress, and it was agreed with the investigation on pre-torsional TiAl alloy, which improved both of strength and ductility [28].

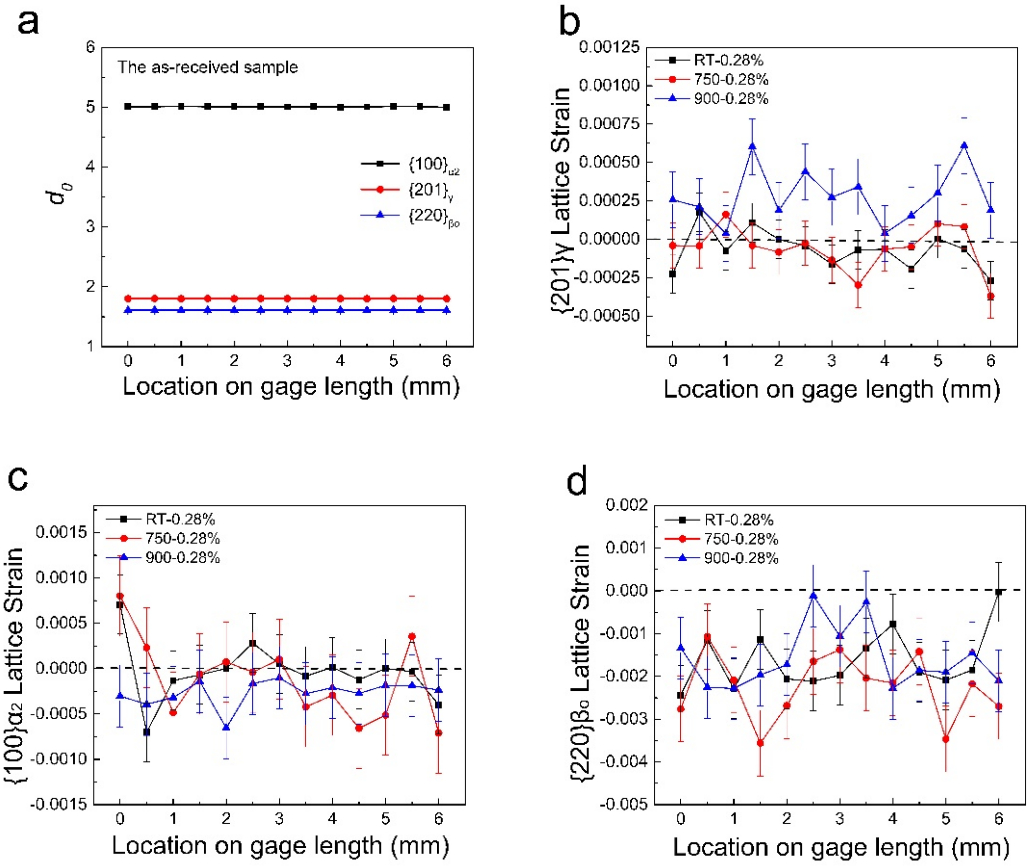

Fig. 4 Distribution of γ, α_2, and β_o residual strains revealed by sample gage length scanning with total strain amplitude of $\Delta\varepsilon_t/2 = \pm 0.28\%$ at room temperature, 750 °C, and 900 °C: (a) the *d0* data taken from the as-received alloy; (b) $\{201\}_{\gamma}$ (c) $\{100\}_{\alpha 2}$; (d) $\{220\}_{\beta o}$.

3.3 Microstructure stability after cyclic deformation at evaluated temperatures

Changes in microstructure after low cycle fatigue with total strain amplitude of $\Delta\varepsilon_t/2 = \pm 0.28\%$ at room temperature, 750 °C, and 900 °C were studied, as showed in Fig. 5a-d. It can be seen that the fully lamellar microstructure of high Nb containing TiAl was mainly destroyed by γ grains and some discontinuous network B2/β_o phases separating along α_2/γ lamellar colony boundaries compared with the as-received fully lamellar microstructure. Grains shown by capital letter A in Fig. 6a and B in Fig. 6b surrounded by α_2/γ lamellar colonies were the recrystallized γ grains which may destroy lamellae structures during cyclic deformation. The γ phase, according to Song ever reported [29],

possesses low stacking fault energy of 80±5 mJ/m^2, which can readily experience discontinuous dynamic recrystallization (DDRX). Dislocations and twins formed during low cycle fatigue can provide the driving force for dynamic recrystallization which becomes the main softening mechanism [30], this was also agreed with the CSS behavior of TiAl alloy cyclic deformed at 750 and 900 °C (Fig. 3). Moreover, γ recrystallized at twin-twin intersection were both observed at 750°C and 900 °C, as well as 850 °C in our previous study [18]. As demonstrated in Fig. 6c, dislocation walls can be found in sample cyclic deformed. It indicated that strain accommodation in recrystallized grains is provided by dislocation glide and climb leading to the formation of sub-grain boundaries. Rearrangement of sub-boundaries may lead to repeated γ recrystallization in recrystallized grains.

Another change on microstructure referred to the phase transformation process. Compared with Fig.5b-d, the α_2/γ lamellar colony size was larger in sample fatigued at room temperature than those cyclic deformed at 750 and 900 °C. This may mainly due to $\gamma \rightarrow \alpha_2$ phase transformation in the recrystallized γ phase and became a new α_2/γ lamellar colony, as showed in Fig. 6a marked by capital letter C. Furthermore, accompanied by $\alpha_2 \rightarrow$ B2 phase transformation (Fig. 5b marked by capital letter D and Fig. 5d marked by capital letter E), the original α_2/γ lamellar colony was destroyed, which may broke into small size colonies. The moving dislocations in the γ phase can be absorbed at the α_2/γ interfaces resulting in the rearrangement of the mismatch interfacial dislocations to accommodate the new interfacial misfit [31]. Then the density of ledges may increase and semi-coherent α_2/γ interfaces were formed. Based on this point, possible lamellar refining mechanisms were proposed for the investigated TiAl alloy low cycle fatigued at 750 and 900 °C. The microstructure degradation of TiAl alloy cyclic deformed at room temperature may mainly resulted from stress-induced $\gamma \rightarrow \alpha_2$ phase transformation process, which also reported by Wang et al. [32].

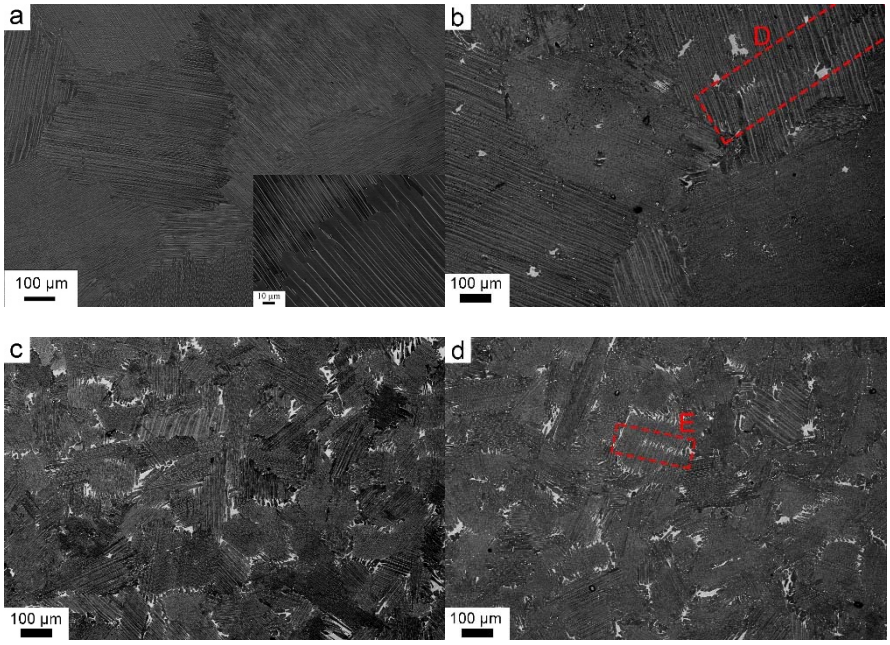

Fig. 5 SEM images of TiAl alloy (a) the as-received fully lamellar microstructure; and after low cycle fatigue with total strain amplitude of $\Delta\varepsilon_t/2 = \pm 0.28\%$ at (b) room temperature; (c) 750 °C; and (d) 900 °C.

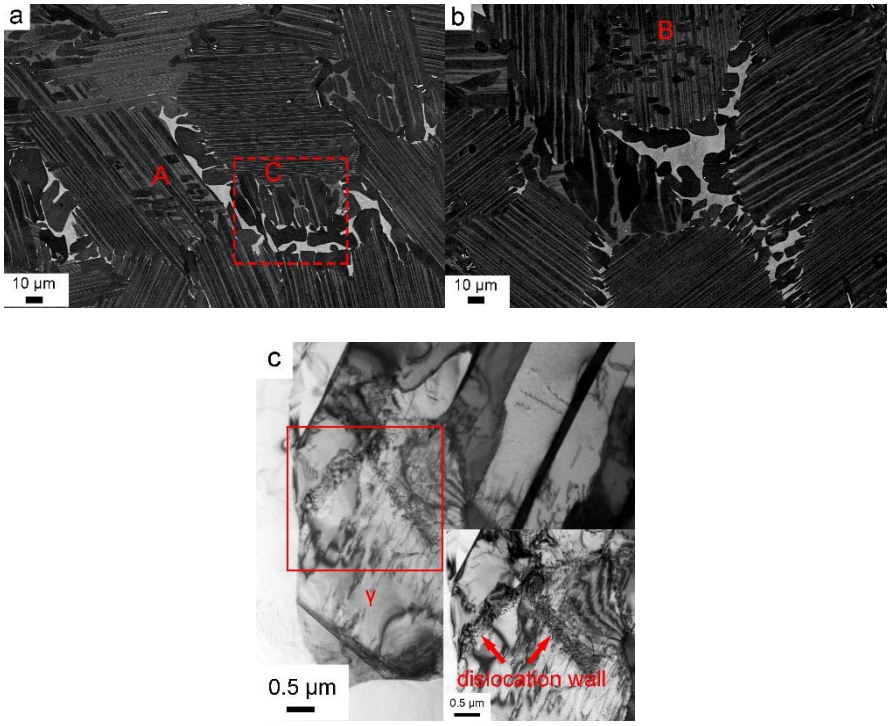

Fig. 6 Magnification SEM images of TiAl alloy after low cycle fatigue with total strain amplitude of $\Delta\varepsilon_t/2 = \pm 0.28\%$ at (a) 750 °C; (b) 900 °C; and TEM bright field observation of dislocation walls at (c) 750 °C.

3.4 Fracture surface examination

Fig. 7a-c shows the fracture morphologies of the as-cast TiAl samples with total strain amplitudes of $\Delta\varepsilon_t/2 = \pm 0.28\%$ after low cycle fatigue tests at room temperature, 750 °C, and 900 °C. After cyclic deformed at room temperature, the fracture surface was relatively smooth and the propagation was mainly interlamellar with some translamellar cracking zones, while fracture surfaces were tough and mainly translamellar after cyclic failed at 750 °C and 900 °C. Besides, the fatigue cracks initiated at the interior of the sample failed at room temperature, whereas samples cyclic deformed at high temperatures, the cracks were preferentially initiated on the surface. Cui et al. [33] have reported that the crack nucleation site was a titanium-rich area, and the hardness of the titanium-rich area was lower than that of the nearby γ and/or α_2 areas, thus fatigue crack preferred to initiate at the titanium-rich area. Furthermore, secondary cracks were widely found between the γ/α_2 lamellar interfaces (Fig. 8a), which was mainly due to the opposite lattice strain directions in γ phase and α_2 phase. The microstructure degradation of γ recrystallization was harmful to TiAl alloy low cycle fatigue deformation, because cracks prefer to propagate along γ grain boundaries (Fig. 8b) due to the stress accumulation caused by tangled dislocations, as showed in Fig. 8c.

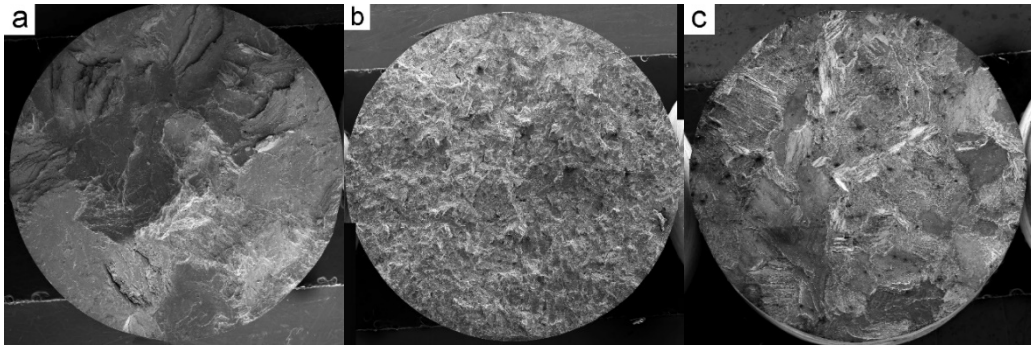

Fig. 7 Fracture surfaces of low cycle fatigue TiAl samples with total strain amplitude of $\Delta\varepsilon_t/2 = \pm 0.28\%$ at (a) room temperature; (b) 750 °C; (c) 900 °C.

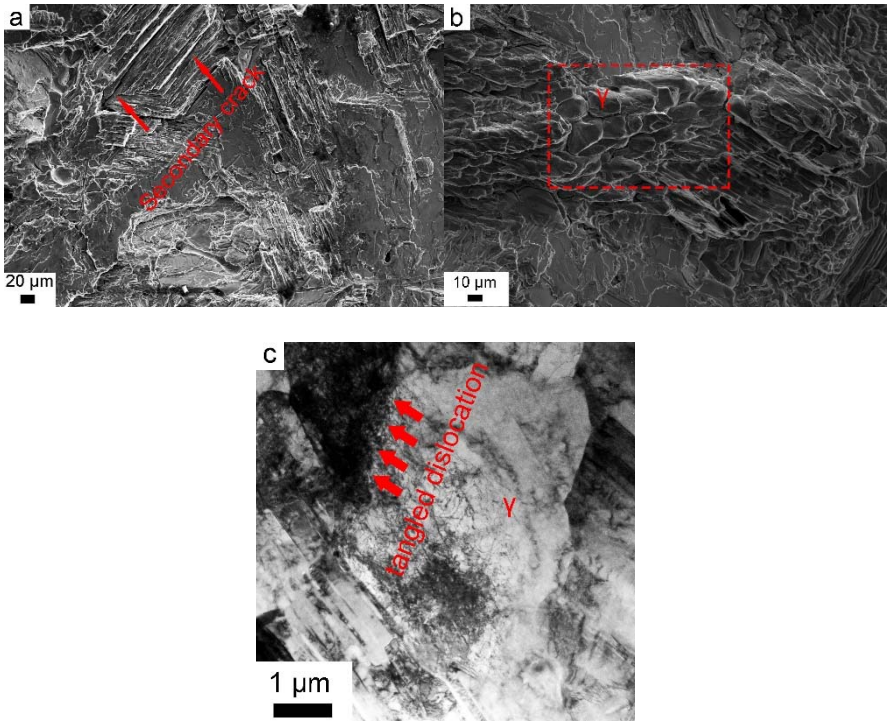

Fig. 8 Fracture morphologies of low cycle fatigue TiAl samples with total strain amplitude of $\Delta\varepsilon_t/2 = \pm 0.28\%$ at 900 °C: (a) secondary crack; (b) crack morphology of γ grains; and (c) TEM image of tangled dislocations at recrystallized γ grain boundary.

4. Conclusions

The low cycle fatigue deformation process in Ti-45Al-8.5Nb-0.2W-0.2B-0.02Y alloy with a fully lamellar microstructure was systematically investigated in this work. The cyclic stress-strain behavior, lattice strains of $\{100\}_{\alpha 2}$, $\{201\}_{\gamma}$, and $\{220\}_{\beta o}$ planes, microstructure stability, and fracture behavior with total strain amplitude of $\Delta\varepsilon_t/2 = \pm 0.28\%$ at room temperature, 750 °C, and 900 °C were discussed. The following conclusions are drawn:

1) The material exhibited cyclic hardening at room temperature while cyclic softening at 750 °C and 900 °C with total strain amplitude of $\Delta\varepsilon_t/2 = \pm 0.28\%$.

2) The different lattice strain directions in γ and α_2 phase resulted in crack propagation along the γ/α_2 interface. The lattice strains in β_o phase were always compressive in the present study and tensile lattice strain in γ phase was detrimental to TiAl low cycle fatigue.

3) The fully lamellar microstructure was mainly destroyed by γ recrystallization and

phase transformations. The process of $\gamma \rightarrow \alpha_2$ phase transformation in the recrystallized γ phase and $\alpha_2 \rightarrow$ B2 phase transformation in the original α_2/γ lamellar colony may be the two reasons proposed for lamellar refinement cyclic deformed at 750 °C and 900 °C. 4) The fatigue fracture mode was mainly interlamellar and crack initiated at sub-surface of the sample cyclic deformed at room temperature, whereas translamellar and crack initiated at surface of the sample cyclic deformed at 750 °C and 900 °C.

Acknowledgements

The authors gratefully acknowledge financial support from the National Natural Science Foundation of China (Project No. 51671016), China Scholarship Council (CSC No. 201908320194, 201908320195), General Program of Natural Science Fund in Colleges and Universities of Jiangsu Province (19KJB430023), Science and technology innovation project for overseas of Nanjing City, Postdoctoral Science Foundation of Jiangsu Province (2019K005), China Postdoctoral Science Foundation (2020M671457, 2019M661781), and Primary Research & Developement Plan of Jiangsu Province (BE2019119). The high energy X-ray experiments were accomplished at Argonne National Laboratory, supported by the US Department of Energy, under Contract No. DE-AC02-06CH11357, and we thank the beam line staffs for assistance in using beam line ID11.

References

[1] Clemens H, Mayer S. Design, processing, microstructure, properties, and applications of advanced intermetallic TiAl alloys[J]. Advanced Engineering Materials, 2013, 15(4): 191-215.

[2] Appel F, Paul J D H, Oehring M. Gamma titanium aluminide alloys: science and technology[M]. John Wiley & Sons, 2011.

[3] Hénaff G, Gloanec A L. Fatigue properties of TiAl alloys[J]. Intermetallics, 2005, 13(5): 543-558.

[4] Wu X. Review of alloy and process development of TiAl alloys[J]. Intermetallics, 2006, 14(10-11): 1114-1122.

[5] Dimiduk D M. Gamma titanium aluminide alloys—an assessment within the competition of aerospace structural materials[J]. Materials Science and Engineering: A,

1999, 263(2): 281-288.

[6] Younas M, Jaffery S H I, Khan M, et al. Multi-objective optimization for sustainable turning Ti6Al4V alloy using grey relational analysis (GRA) based on analytic hierarchy process (AHP)[J]. The International Journal of Advanced Manufacturing Technology, 2019, 105(1-4): 1175-1188.

[7] Klein T, Clemens H, Mayer S. Advancement of compositional and microstructural design of intermetallic γ-TiAl based alloys determined by atom probe tomography[J]. Materials, 2016, 9(9): 755.

[8] Liu H, Li Z, Gao F, et al. High tensile ductility and strength in the Ti-42Al-6V-1Cr alloy[J]. Journal of Alloys and Compounds, 2017, 698: 898-905.

[9] Chen G, Peng Y, Zheng G, et al. Polysynthetic twinned TiAl single crystals for high-temperature applications[J]. Nature Materials, 2016, 15(8): 876-881.

[10] Kim S W, Hong J K, Na Y S, et al. Development of TiAl alloys with excellent mechanical properties and oxidation resistance[J]. Materials & Design (1980-2015), 2014, 54: 814-819.

[11] Zhao W, Pei Y, Zhang D, et al. The microstructure and tensile property degradation of a gamma-TiAl alloy during isothermal and cyclic high temperature exposures[J]. Intermetallics, 2011, 19(3): 429-432.

[12] Appel F, Heckel T K, Christ H J. Electron microscope characterization of low cycle fatigue in a high-strength multiphase titanium aluminide alloy[J]. International Journal of Fatigue, 2010, 32(5): 792-798.

[13] Kruml T, Obrtlík K. Microstructure degradation in high temperature fatigue of TiAl alloy[J]. International Journal of Fatigue, 2014, 65: 28-32.

[14] Ding J, Liang Y, Xu X, et al. Cyclic deformation and microstructure evolution of high Nb containing TiAl alloy during high temperature low cycle fatigue[J]. International Journal of Fatigue, 2017, 99: 68-77.

[15] Gloanec A L, Henaff G, Bertheau D. Influence of temperature on the low cycle fatigue behaviour of a gamma-titanium-aluminide alloy[M]//European Structural Integrity Society. Elsevier, 2002, 29: 103-112.

[16] Umakoshi Y, Yasuda H Y, Nakano T. Plastic anisotropy and fatigue of TiAl PST

crystals: a review[J]. Intermetallics, 1996, 4: S65-S75.

[17] Gloanec A L, Jouiad M, Bertheau D, et al. Low-cycle fatigue and deformation substructures in an engineering TiAl alloy[J]. Intermetallics, 2007, 15(4): 520-531.

[18] Ding J, Zhang M, Ye T, et al. Microstructure stability and micro-mechanical behavior of as-cast gamma-TiAl alloy during high-temperature low cycle fatigue[J]. Acta Materialia, 2018, 145: 504-515.

[19] Wang X, Yang J, Song L, et al. Evolution of B2 (ω) region in high-Nb containing TiAl alloy in intermediate temperature range[J]. Intermetallics, 2017, 82: 32-39.

[20] Ye T, Song L, Gao S, et al. Precipitation behavior of the ω_o phase in an annealed high Nb-TiAl alloy[J]. Journal of Alloys and Compounds, 2017, 701: 882-891.

[21] Gao S, Xu X, Shen Z, et al. Microstructure and properties of forged plasma arc melted pilot ingot of Ti-45Al-8.5Nb-(W, B, Y) alloy[J]. Materials Science and Engineering: A, 2016, 677: 89-96.

[22] Xu X, Lin J, Guo J, et al. Microstructure and properties of friction welding joint of Ti-45Al-8.5 Nb-0.2W-0.2B-0.02Y alloy[J]. Intermetallics, 2019, 112: 106540.

[23] Gloanec A L, Henaff G, Jouiad M, et al. Cyclic deformation mechanisms in a gamma titanium aluminide alloy at room temperature[J]. Scripta Materialia, 2005, 52(2): 107-111.

[24] Jouiad M, Gloanec A L, Grange M, et al. Cyclic deformation mechanisms in a cast gamma titanium aluminide alloy[J]. Materials Science and Engineering: A, 2005, 400: 409-412.

[25] Withers P J, Bhadeshia H. Residual stress. Part 2-Nature and origins[J]. Materials Science and Technology, 2001, 17(4): 366-375.

[26] Roland T, Retraint D, Lu K, et al. Fatigue life improvement through surface nanostructuring of stainless steel by means of surface mechanical attrition treatment[J]. Scripta Materialia, 2006, 54(11): 1949-1954.

[27] Ortiz A L, Tian J W, Villegas J C, et al. Interrogation of the microstructure and residual stress of a nickel-base alloy subjected to surface severe plastic deformation[J]. Acta Materialia, 2008, 56(3): 413-426.

[28] Ding J, Zhang M, Liang Y, et al. Enhanced high-temperature tensile property by

gradient twin structure of duplex high-Nb-containing TiAl alloy[J]. Acta Materialia, 2018, 161: 1-11.

[29] Song X P, Chen G L. Effect of elastic anisotropy on the dissociation widths of superdislocations in TiAl[J]. Materials Letters, 2001, 48(5): 273-280.

[30] Zhang S Z, Kong F T, Chen Y Y, et al. Phase transformation and microstructure evolution of differently processed Ti-45Al-9Nb-Y alloy[J]. Intermetallics, 2012, 31: 208-216.

[31] Wang J G, Ph.D. Thesis, University of Science and Technology Beijing, Beijing, 1994.

[32] Wang J G, Chen G L, Zhang L C, et al. Study on the stress-induced γ → α2 transformation in a hot-deformed Ti-45Al-10Nb alloy by high-resolution transmission electron microscopy[J]. Materials Letters, 1997, 31(3-6): 179-183.

[33] Cui W F, Liu C M. Fracture characteristics of γ-TiAl alloy with high Nb content under cyclic loading[J]. Journal of Alloys and Compounds, 2009, 477(1-2): 596-601.